ADVANCES IN ATMOSPHERIC SCIENCES, VOL. 29, NO. 6, 2012, 1343–1359

Kinetic and Available Potential Energy Transport during the Stratospheric Sudden Warming in January 2009

ZUO Qunjie[1,2,3] (左群杰), GAO Shouting*[1,4] (高守亭), and LÜ Daren[3] (吕达仁)

[1] *Laboratory of Cloud-Precipitation Physics and Severe Storms, Institute of Atmospheric Physics, Chinese Academic of Sciences, Beijing* 100029

[2] *Graduate University of Chinese Academic of Sciences, Beijing* 100029

[3] *Key Laboratory of Middle Atmosphere and Global Environment Observation, Institute of Atmospheric Physics, Chinese Academic of Sciences, Beijing* 100029

[4] *State Key Laboratory of Severe Weather, Chinese Academy of Meteorological Sciences, Beijing* 100029

(Received 12 October 2011; revised 11 January 2012)

ABSTRACT

The local features of transient kinetic energy and available potential energy were investigated using ECMWF (European Centre for Medium-Range Weather Forecasts) Interim Reanalysis data for the stratospheric sudden warming (SSW) event of January 2009. The Western Europe high plays important roles in the propagation of the energy from North America to Eurasian. When the Western Europe high appeared and shifted eastward, energy conversions increased and energy propagated from North America to Eurasian as a form of interaction energy flow. The baroclinic conversion between transient-eddy kinetic energy (K_e) and transient-eddy available potential energy (A_e) and the horizontal advection of geopotential height were approximately one order of magnitude less than K_e and A_e generation terms. So, these terms were less important to this SSW event.

Key words: energy flow, energy conversion, kinetic energy, APE, stratospheric sudden warming

Citation: Zuo, Q. J., S. T. Gao, and D. R. Lü, 2012: Kinetic and available potential energy transport during the stratospheric sudden warming in January 2009. *Adv. Atmos. Sci.*, **29**(6), 1343–1359, doi: 10.1007/s00376-012-1198-5.

1. Introduction

In the second half of January 2009, a prominent stratospheric sudden warming (SSW) occurred in the Northern Hemisphere. The SSW was a sudden breakdown of the polar vortex caused by dynamical forcing of upward-propagation planetary waves from the troposphere (Andrews et al., 1987). This is a very sporadic phenomenon that does not occur every winter. Some SSWs primarily involve planetary wavenumber 2, while others involve an enhancement of wavenumber 1. According to the classification of World Meteorological Organization, a major warming or SSW is defined as follows: at $\leqslant$10 hPa in the stratosphere, the zonal mean temperature increases poleward from 60° latitude and the zonal mean zonal wind reverses. A minor warming is defined as follows: the temperature gradient reverses but the zonal mean zonal wind does not. According to these definitions, the event during the second half of January 2009 was a major warming event. The essential dynamic mechanism responsible for sudden warming is the upward propagation from the troposphere of planetary waves and their interaction with the mean stratospheric flow. This hypothesis was first proposed by Matsuno (1971). The observed characteristics of various warmings are described in a number of papers (e.g., Holton and Tan, 1980; Labitzke, 1982, 1987; Labitzke and van Loon, 1992, 1999; Baldwin and Dunkerton, 2001; Mukougawa et al., 2005; Labitzke et al., 2006; Nakagawa

*Corresponding author: GAO Shouting, gst@mail.iap.ac.cn

and Yamazaki, 2006; Hirooka et al., 2007; Kuroda, 2008; Harada et al., 2010). The energy cycle of the SSW has also been the subject of a number of studies (e.g., Reed et al., 1963; Murakami, 1965; Julian and Labitzke, 1965; Muench, 1965; Perry, 1967). All of these studies analyzed the energy budget of the SSW in terms of the Lorenz cycle of energy conversions, basically with a global view. If we consider the local energy balance by dividing basic variables into time-mean and transient-eddy components using the Lorenz diagram, we are faced with some ambiguity in the interpretation of which terms in the energy equations for an open system represent an energy conversion from one to another (Holopainen, 1978; Plumb, 1983). Recently, Murakami (2011) reconstructed the classical energetics analysis based on the concept of interaction energy and its flux to solve the question raised by Holopainen (1978).

In this paper, we show the features of the SSW that occurred in January 2009 from the viewpoint of local energy conversion. The data and analysis are described in section 2. In section 3, the eddy available potential energy budget during the SSW is discussed. The local features of kinetic energy during the SSW are presented in section 4. The conclusions are presented in section 5.

2. Data and analysis

This study is based on the 6-hourly ECMWF (European Centre for Medium-Range Weather Forecasts) Interim Reanalysis data (ERA-Interim, Simmons et al., 2007) for 2009. The ERA-Interim data (ECMWF Interim Reanalysis data) have a 1.5°×1.5° horizontal resolution and 37 pressure levels from 1000 to 1 hPa. The data have a T255 horizontal resolution with 60 vertical hybrid levels for the spectral model. A data assimilation system (4-dimensional variational) with 12-h cycling is used with output every 6 h. A new humidity analysis has been included in the assimilation. Variational bias correction of satellite radiance data and other improvements were performed before assimilation.

The standard momentum, hydrostatic, thermodynamic, and continuity equations for a dry atmosphere in the spherical pressure coordinates system can be written as follows (e.g., Murakami, 2011):

$$\frac{\partial u}{\partial t}+\frac{u}{a\cos\varphi}\frac{\partial u}{\partial \lambda}+\frac{v}{a}\frac{\partial u}{\partial \varphi}+\omega\frac{\partial u}{\partial p}-\frac{\tan\varphi}{a}uv-fv$$

$$=-\frac{1}{a\cos\varphi}\frac{\partial \phi}{\partial \lambda}+F_\lambda, \tag{1a}$$

$$\frac{\partial v}{\partial t}+\frac{u}{a\cos\varphi}\frac{\partial v}{\partial \lambda}+\frac{v}{a}\frac{\partial v}{\partial \varphi}+\omega\frac{\partial v}{\partial p}+\frac{\tan\varphi}{a}uu+fu$$

$$=-\frac{1}{a}\frac{\partial \phi}{\partial \varphi}+F_\varphi\,, \tag{1b}$$

$$0=-\frac{\partial \phi}{\partial p}-\alpha\,, \tag{1c}$$

$$\frac{\partial \theta}{\partial t}+\frac{u}{a\cos\varphi}\frac{\partial \theta}{\partial \lambda}+\frac{v}{a}\frac{\partial \theta}{\partial \varphi}+\omega\frac{\partial \theta}{\partial p}=\left(\frac{p_0}{p}\right)^\kappa\frac{Q}{c_p}\,, \tag{1d}$$

$$\frac{1}{a\cos\varphi}\frac{\partial u}{\partial \lambda}+\frac{1}{a\cos\varphi}\frac{\partial v\cos\varphi}{\partial \varphi}+\frac{\partial \omega}{\partial p}=0\,, \tag{1e}$$

where λ is longitude, φ is latitude, p is pressure, t is time, $(u,\ v)$ is eastward and northward wind speed respectively, ω is pressure velocity, ϕ is geopotential height, a is the radius of the earth, f is the Coriolis parameter, F=(F_λ, F_φ, 0) is horizontal friction force, Q is diabatic heating, p_0 is reference pressure (=1000 hPa), c_p is atmospheric specific heat at constant pressure, κ is the ratio of the gas constant and specific heat ($=R/c_p$), θ is potential temperature [$=T(p/p_0)^\kappa$, where T is temperature], and α is specific volume ($=RT/p$).

To study the time evolution of the energy budget, the basic variables u, v, ω, ϕ and θ were divided into two components ($u=u_\mathrm{m}+u_\mathrm{e}$), where the subscript m indicates 23 years of average daily January values from the 1989 to 2011 data of ERA-Interim and the subscript e denotes the deviation from this time mean. In this case, the kinetic energy per unit mass is given by

$$K=\frac{u_\mathrm{m}^2+v_\mathrm{m}^2}{2}+\frac{u_\mathrm{e}^2+v_\mathrm{e}^2}{2}+(u_\mathrm{m}u_\mathrm{e}+v_\mathrm{m}v_\mathrm{e})$$
$$=K_\mathrm{m}+K_\mathrm{e}+K_\mathrm{i}\,, \tag{2}$$

where K_m, K_e, and K_i are the kinetic energy densities for the mean flow, the transient-eddy field, and the interaction kinetic energy density (Murakami, 2011), respectively. The available potential energy (APE) per unit mass is given by

$$A=\frac{c_p}{2}\left(\frac{p}{p_0}\right)^{2\kappa}\gamma(\theta_\mathrm{m}-\widetilde{\theta})^2+\frac{c_p}{2}\left(\frac{p}{p_0}\right)^{2\kappa}\gamma\theta_e^2+$$
$$\frac{c_p}{2}\left(\frac{p}{p_0}\right)^{2\kappa}\gamma\theta_\mathrm{e}(\theta_\mathrm{m}-\widetilde{\theta})$$
$$=A_\mathrm{m}+A_\mathrm{e}+A_\mathrm{i}\,, \tag{3}$$

where A_m, A_e, and A_i are the time mean, transient-eddy and interaction components (Murakami, 2011) of APE density A, respectively. Here

$$\gamma=-(\kappa/p)(p_0/p)^\kappa(d\widetilde{\theta}/dp)^{-1}\,,$$

is the static stability index of dry atmosphere, and $\widetilde{\ }$ denotes the global-average operator in this coordinate

system. Following Murakami (2011), the transient kinetic energy equation is [see Eq. (10) in Murakami, 2011]

$$\begin{aligned}&\frac{\partial}{\partial t}(K_{\rm e})+\boldsymbol{V}_{\rm m}\cdot\nabla(K_{\rm e})+\boldsymbol{V}_{\rm e}\cdot\nabla(K_{\rm e})\\&=-\boldsymbol{V}_{\rm e}\cdot\nabla\phi_{\rm e}-\omega_{\rm e}\alpha_{\rm e}-[u_{\rm e}\boldsymbol{V}_{\rm e}\cdot\nabla u_{\rm m}+\\&v_{\rm e}\boldsymbol{V}_{\rm e}\cdot\nabla v_{\rm m}+\frac{\tan\varphi}{a}(u_{\rm m}u_{\rm e}v_{\rm e}-v_{\rm m}u_{\rm e}u_{\rm e})]+\\&u_{\rm e}\nabla\times(u_{\rm e}\boldsymbol{V}_{\rm e})_{\rm m}+v_{\rm e}\nabla\times(v_{\rm e}\boldsymbol{V}_{\rm e})_{\rm m}-\\&\frac{\tan\varphi}{a}[u_{\rm e}(u_{\rm e}v_{\rm e})_{\rm m}-v_{\rm e}(u_{\rm e}u_{\rm e})_{\rm m}]+F\,,\end{aligned}\tag{4}$$

The divergence and gradient operators in this coordinate system can be expressed as

$$\nabla\cdot\boldsymbol{V}=\frac{1}{a\cos\varphi}\frac{\partial u}{\partial\lambda}+\frac{1}{a\cos\varphi}\frac{\partial v\cos\varphi}{\partial\varphi}+\frac{\partial\omega}{\partial p}=0,\tag{5}$$

$$\boldsymbol{V}\cdot\nabla=\frac{u}{a\cos\varphi}\frac{\partial}{\partial\lambda}+\frac{v}{a}\frac{\partial}{\partial\varphi}+\omega\frac{\partial}{\partial p}\,,\tag{6}$$

where $\boldsymbol{V}$=(u, v, ω) is the three-dimensional wind. The terms on the left-hand side of Eq. (4) are the local transient kinetic energy tendency, the advection by the mean flow, and the advection by the transient-eddies. The first term on the right-hand side of Eq. (4) is the transient geopotential height advection by the transient eddies. The second term is commonly interpreted as the conversion rate from transient available potential to transient kinetic energy. The third term in the bracket is a part of interaction energy flux of kinetic energy when it is properly averaged in time, which could be interpreted as energy conversion rate form $K_{\rm e}$ to $K_{\rm i}$ (see express C_2 in Murakami, 2011). The remaining terms on the right-hand side of Eq. (4) could not be calculated directly and be regarded as the residue of other terms mentioned above. These terms will not be contained in the text.

The transient available potential energy equation is [taking Eq. (19) in Murakami, 2011 and multiplying by $c_p(p/p_0)^{2\kappa}\gamma$,

$$\begin{aligned}&\frac{\partial}{\partial t}\left[c_p(p/p_0)^{2\kappa}\gamma\frac{\theta_{\rm e}^2}{2}\right]+c_p(p/p_0)^{2\kappa}\gamma\left[\boldsymbol{V}_{\rm m}\cdot\right.\\&\left.\nabla\left(\frac{\theta_{\rm e}^2}{2}\right)+\boldsymbol{V}_{\rm e}\cdot\nabla\left(\frac{\theta_{\rm e}^2}{2}\right)\right]\\&=-c_p(p/p_0)^{2\kappa}\gamma\omega_{\rm e}\theta_{\rm e}\frac{\partial\widetilde{\theta}}{\partial p}-c_p(p/p_0)^{2\kappa}\gamma\theta_{\rm e}\boldsymbol{V}_{\rm e}\cdot\\&\nabla(\theta_{\rm m}-\widetilde{\theta})+c_p(p/p_0)^{2\kappa}\gamma\frac{p_0}{p}\frac{\theta_{\rm e}Q_{\rm e}}{c_p}+\\&c_p(p/p_0)^{2\kappa}\gamma\theta_{\rm e}\nabla\times(\theta_{\rm e}\boldsymbol{V}_{\rm e})_{\rm m}\,.\end{aligned}\tag{7}$$

The terms on the left-hand side of Eq. (7) are the local transient APE tendency, the advection by the mean flow, and the advection by the transient-eddies. The first term on the right-hand side of Eq. (7) is the conversion rate from transient kinetic energy to transient available potential. The second term is a part of the interaction energy flux of APE when it is properly averaged over time, which could be interpreted as energy conversion rate from $A_{\rm e}$ to $A_{\rm i}$ [see express $C(A_T,\,A_I)$ in Murakami, 2011]. The residual terms are discussed together and are considered as the residue of other terms. These terms are not contained in this text.

In the calculation of the different terms in Eqs. (4) and (7), a vertical average is defined as

$$\widehat{A}=\frac{1}{p_{\rm s}-p_{\rm t}}\int_{p_{\rm t}}^{p_{\rm s}}A dp\,,$$

where $p_{\rm s}$ and $p_{\rm t}$ are 100 hPa and 10 hPa, respectively. The integration is done using the trapezoidal method. Unless otherwise stated, the plots are shown as vertical integration, with the hat dropped for simplicity of notation.

3. Time evolution of the transient kinetic energy and its budget

Before discussing the variation of transient kinetic energy ($K_{\rm e}$), we first describe some basic feature of the atmospheric circulation during the warming of January 2009. Figure 1 shows the distribution of 10-hPa geopotential for 2-day intervals between 9 and 25 January. At the beginning of the warming (Figs. 1a–1c), the basic cyclone polar vortex is located over the North Pole, with both a trough over North America and the Aleutian High being present. During the period between 15 and 17 January (Figs. 1a–1c), another high over Western Europe and a trough over central Siberia also began to develop. During 19–23 January (Figs. 1f–1h), with the trough over North America and central Siberia and the highs over Western Europe and Aleutian developing, the polar vortex split into two cyclones. On 25 January (Fig. 1i), one of the cyclones shifted southward toward the north of Great Lakes and the high over Western Europe shifted westward. More detailed features of the warming can be found in Harada et al. (2010).

A sequence of the vertical averaged local tendencies of $K_{\rm e}$ and the 10-hPa geopotential are shown in Fig. 2 for 48-h intervals between 9 and 25 January. This period includes the sudden warming of 23 January. Before commenting on the major warming itself, distinguishing features of this period were the eastward development of the $K_{\rm e}$ and trough. The positive values denote the growth of $K_{\rm e}$, and the negative values denote the decay of $K_{\rm e}$. Rapid-phase eastward pro-

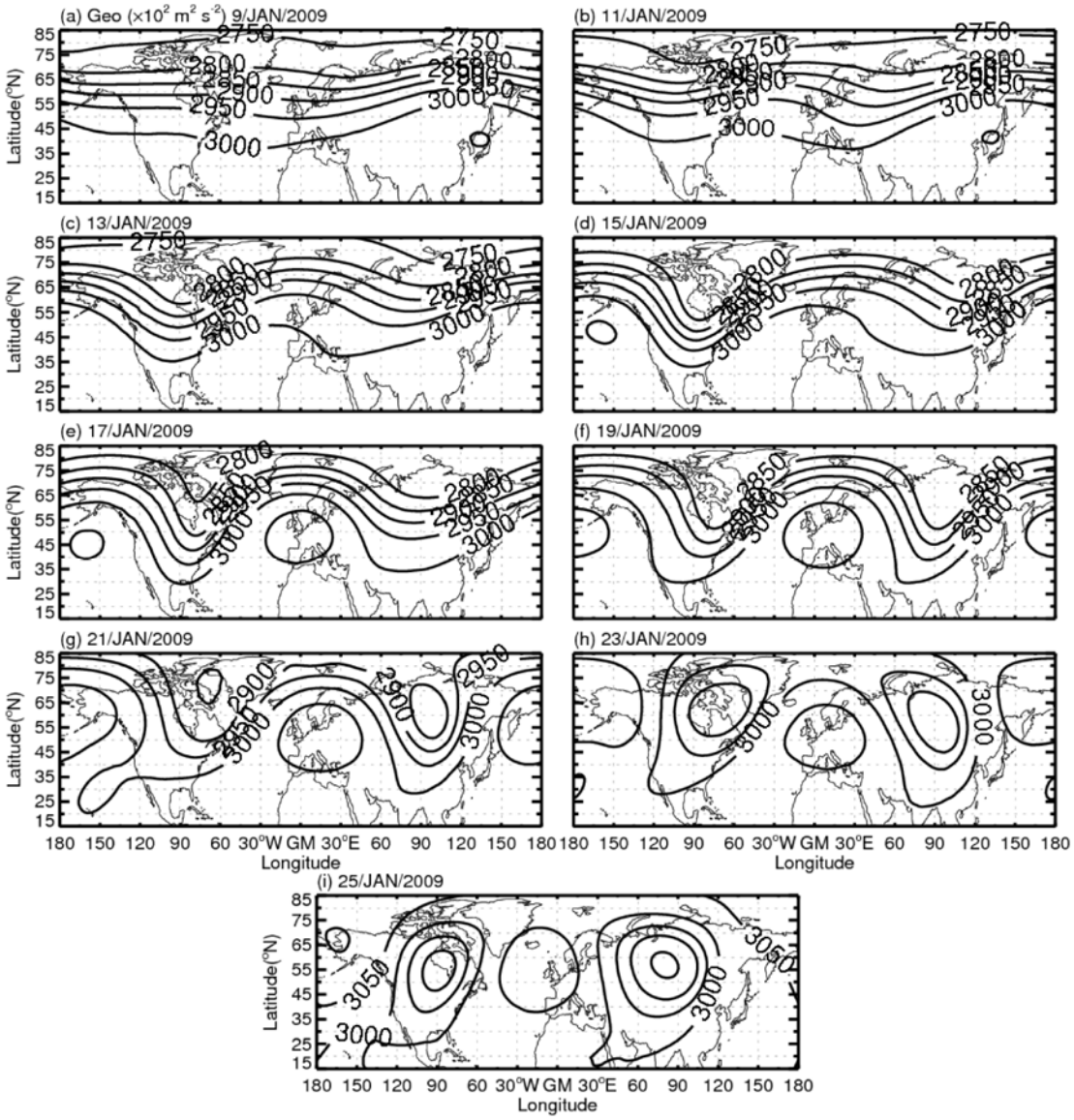

Fig. 1. The 10-hPa geopotential at 48-h intervals from 9 to 25 January 2009. The contour interval is 50×10^2 m^2 s^{-2}.

gression of K_e and trough were observed from 9 to 21 January. For instance, a positive center over Alaska increased and shifted eastward to central Canada from 9 to 17 January (Figs. 2a–e), then shifted eastward continually but quickly decreased from 17 to 21 January (Figs. 2e–g). The other positive center over eastern Canada increased from 9 to 15 January (Figs. 2a–d), then decreased and shifted eastward to Eastern Europe and then to Russia and to northeastern China from 15 to 21 January (Figs. 2d–g). For the two continents, asymmetric variations of K_e and trough can be seen. These characteristics indicate that the variation of K_e and the development of trough were cumulative, which is consistent with the behavior of the upward propagation of stationary wave from troposphere during January 2009 (Harada et al., 2010).

One of the principal reason of the major warming was the upward propagation of wavenumber 2 (Matsuno, 1971; Palmer, 1981) and this upward propagation was cumulative (Harada et al., 2010). The eastward propagation of the vortex based on isentropic potential vorticity prior to the warming also seems to be important (Dunkerton and Delisi, 1986). On the basis of the observation in Fig. 2, the rapid development of the local tendencies of K_e prior to the warming is also significant.

Next, using the interaction energy theory introduced by Murakami (2011), we examined the transport, sources, and sinks associated with the K_e and transient available potential energy (A_e, see next sec-

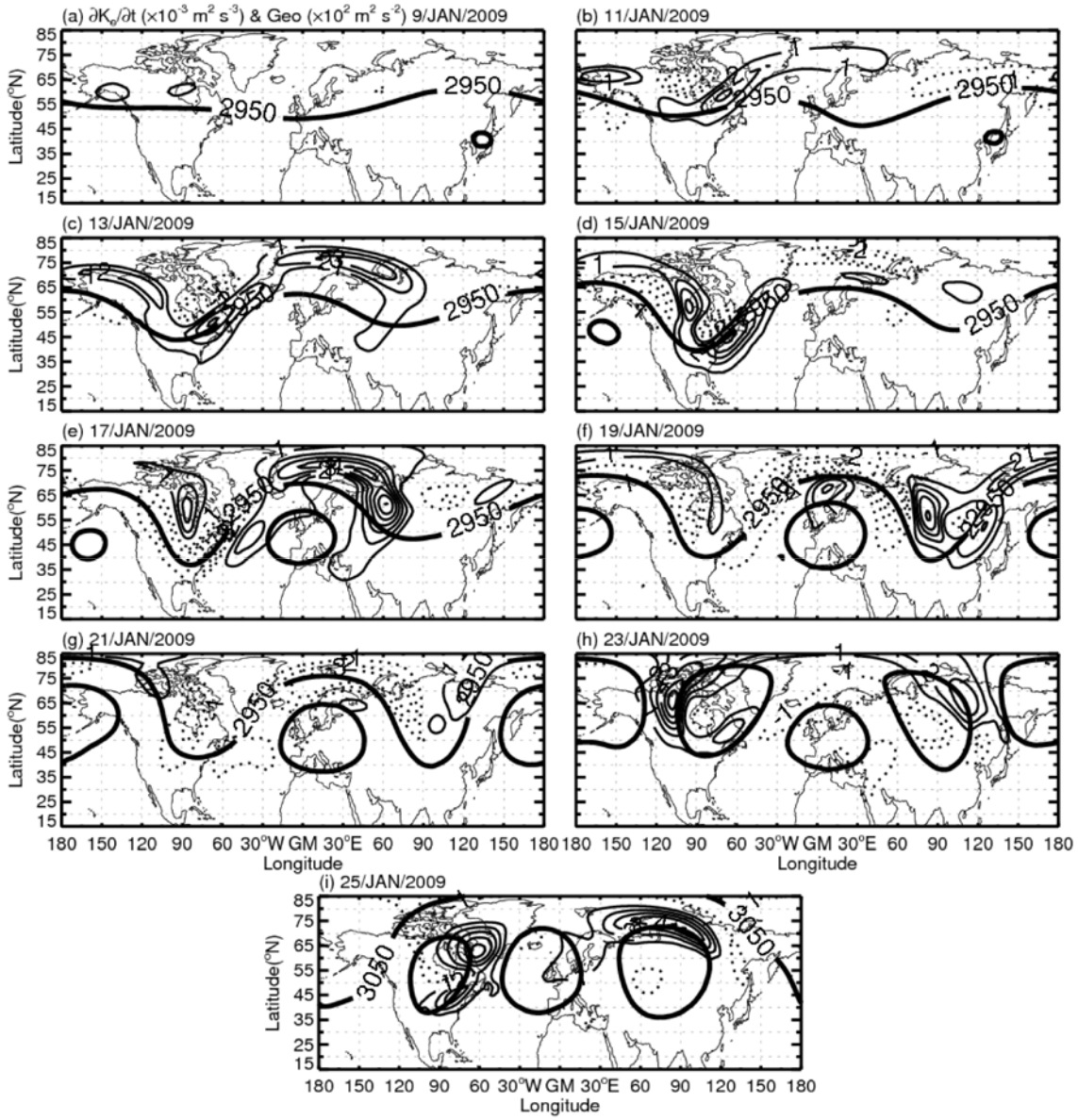

Fig. 2. Vertically averaged local tendencies of transient kinetic energy at 48-h intervals from 9 to 25 January 2009. The solid lines denote positive values and the dotted lines denote negative values. Contour interval is 1×10^{-3} m^2 s^{-3}. The contour of zero value is omitted. The geopotential values of 2950×10^2 m^2 s^{-2} and 3050×10^2 m^2 s^{-2} on 10 hPa are denoted by thick solid lines.

tion), and we found a relationship with the variation of the SSW. The K_e budget of this warming was analyzed by applying ERA-Interim data to Eq. (4). The gross behavior of local tendencies can be explained by the advection of K_e by both the mean and the transient wind. The advection by transient wind is shown in Fig. 3. The polarward advection by the transient wind is clearly evident. This transient advection appeared over North America and increased from 9 to 15 January (Figs. 3a–d), then through the Norwegian Sea into North Eurasia and increased from 15 to 19 January over northern Eurasia (Figs. 3d–f). Before the major warming from 19 to 21 January (Figs. 3f–g), the transient advection decreased over both continents. After the major warming event from 23 to 25 January (Figs. 3h–i), the advection by the transient wind over two continents obviously changed its direction from polarward to eastward. The advection by mean wind is shown in Fig. 4. The eastward advection due to the mean wind can be clearly seen. The variation of this mean advection was also connected with location. The mean advection shifts eastward and increased from 9 to 15 January over northern North America (Figs. 4a–d), then through the Norwegian Sea

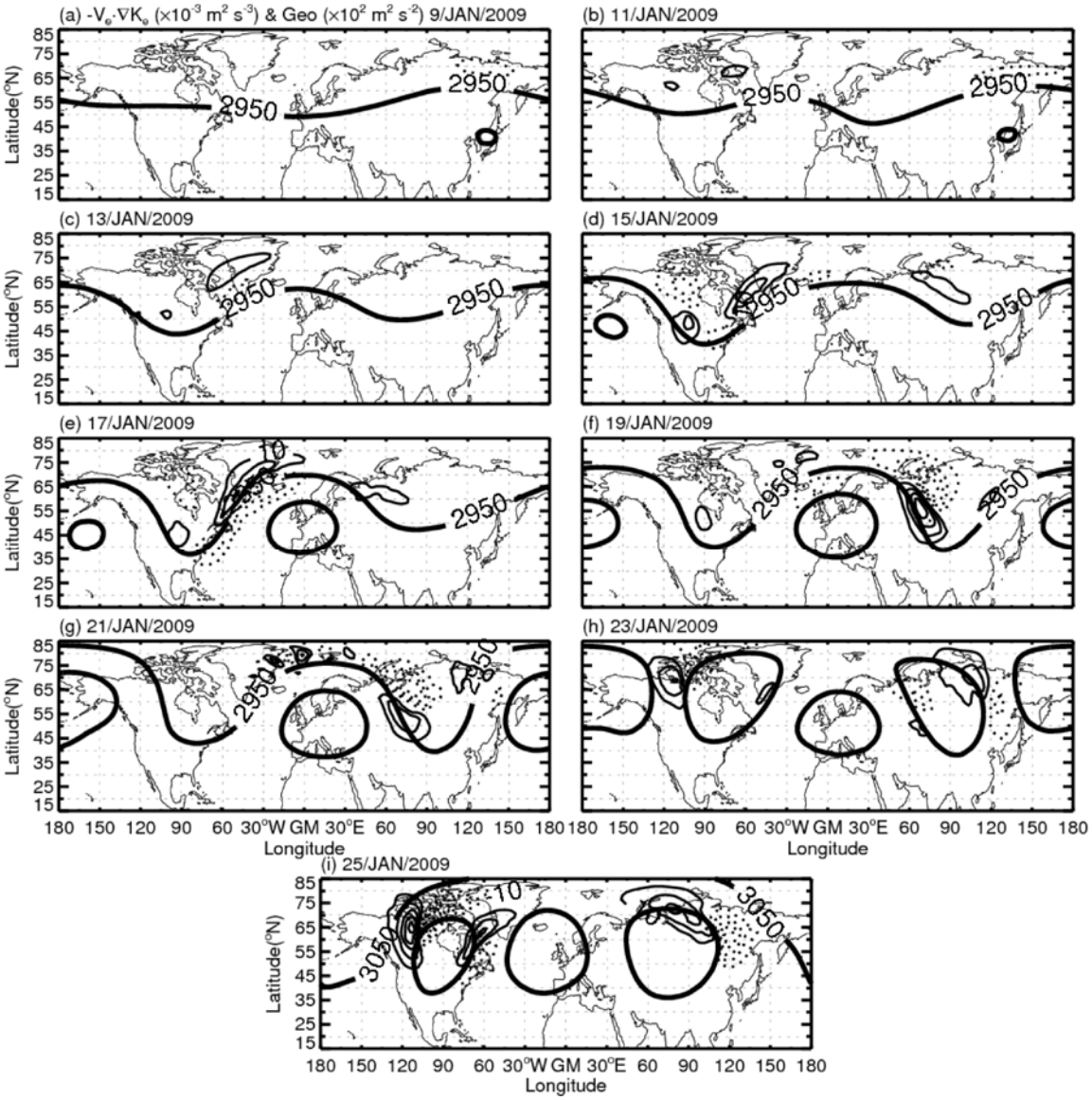

Fig. 3. Vertically averaged transient kinetic energy advection by transient flow at 48-h intervals from 9 to 25 January 2009. The solid lines denote positive values and the dotted lines denote negative values. Contour interval is 10×10^{-3} m^2 s^{-3}. The contour of zero value is omitted. The geopotential values of 2950×10^2 m^2 s^{-2} and 3050×10^2 m^2 s^{-2} on 10 hPa are denoted by thick solid lines.

into northern Eurasia and increased from 15 to 19 January over northern Eurasia (Figs. 4d–f). Prior to the major warming from 19 to 21 January (Figs. 4f–g), the mean advection decreased over both continents. After major warming from 23 to 25 January (Figs. 4h–i), the eastward advection by mean wind increased over two continents. Comparing Fig. 3 with Fig. 4, the transient advection was of the same order as the mean advection of K_e, whereas commonly the transient advection of K_e was assumed to be a third-order quantity. For the case of the warming event in January 2009, this result may have been true. When transient and mean advection terms were integrated over a sufficient length of time, the magnitude of transient advection was possibly smaller than that of mean advection. Notably, the contributions of these two terms to the local tendencies of K_e largely cancelled when integrated over the entire atmosphere. If so, the net tendencies were determined more by the remaining terms in Eq. (4).

K_e generation term $-\boldsymbol{V}_e \cdot \nabla\phi_e$ and baroclinic conversion $-\omega_e\alpha_e$ represent a conversion between A_e and K_e. They are related by

$$-\boldsymbol{V}_e \cdot \nabla\phi_e - \omega_e\alpha_e = -\left(\frac{u_e}{a\cos\varphi}\frac{\partial\phi_e}{\partial\lambda} + \frac{v_e}{a}\frac{\partial\phi_e}{\partial\varphi}\right). \quad (8)$$

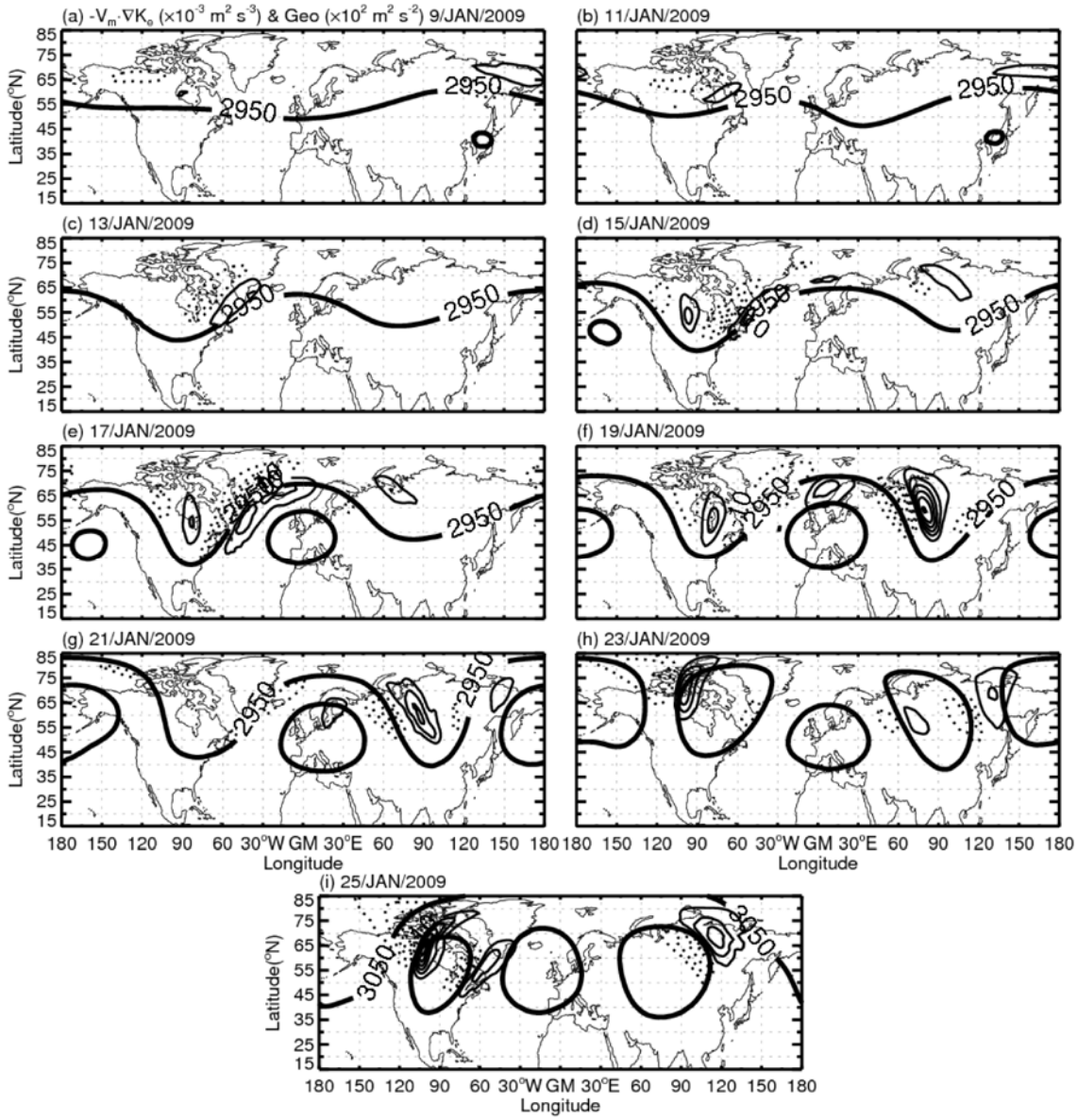

Fig. 4. Vertically averaged transient kinetic energy advection by mean flow at 48-h intervals from 9 to 25 January 2009. The solid lines denote positive values and the dotted lines denote negative values. Contour interval is 10×10^{-3} m^2 s^{-3}. The contour of zero value is omitted. The geopotential values of 2950×10^2 m^2 s^{-2} and 3050×10^2 m^2 s^{-2} on 10 hPa are denoted by thick solid lines.

The quantity on the right-hand side of Eq. (8) is plotted in Fig. 5. The generation of transient kinetic energy was approximately one order of magnitude less than the advection terms, and the term from 17 to 25 January is shown in Fig. 5. The growth and decay of K_e appeared over North America on 15 January (Fig. 5a). The extent of the variation of K_e decreased from 15 to 21 January over North America (Figs. 5a–5d). With this decreasing, the growth and decay of K_e obviously appeared over Eurasia on 19 January then decreased. This K_e generation term was too small to explain the behavior of the local tendencies during this SSW event.

There is another K_e generation term

$$-\left[u_\mathrm{e}\boldsymbol{V}_\mathrm{e}\cdot\nabla u_\mathrm{m}+v_\mathrm{e}\boldsymbol{V}_\mathrm{e}\cdot\nabla v_\mathrm{m}+\frac{\tan\varphi}{a}(u_\mathrm{m}u_\mathrm{e}v_\mathrm{e}-v_\mathrm{m}u_\mathrm{e}u_\mathrm{e})\right]. \quad (9)$$

There is some ambiguity in the interpretation of this term in the energy equation for an open system (Holo-

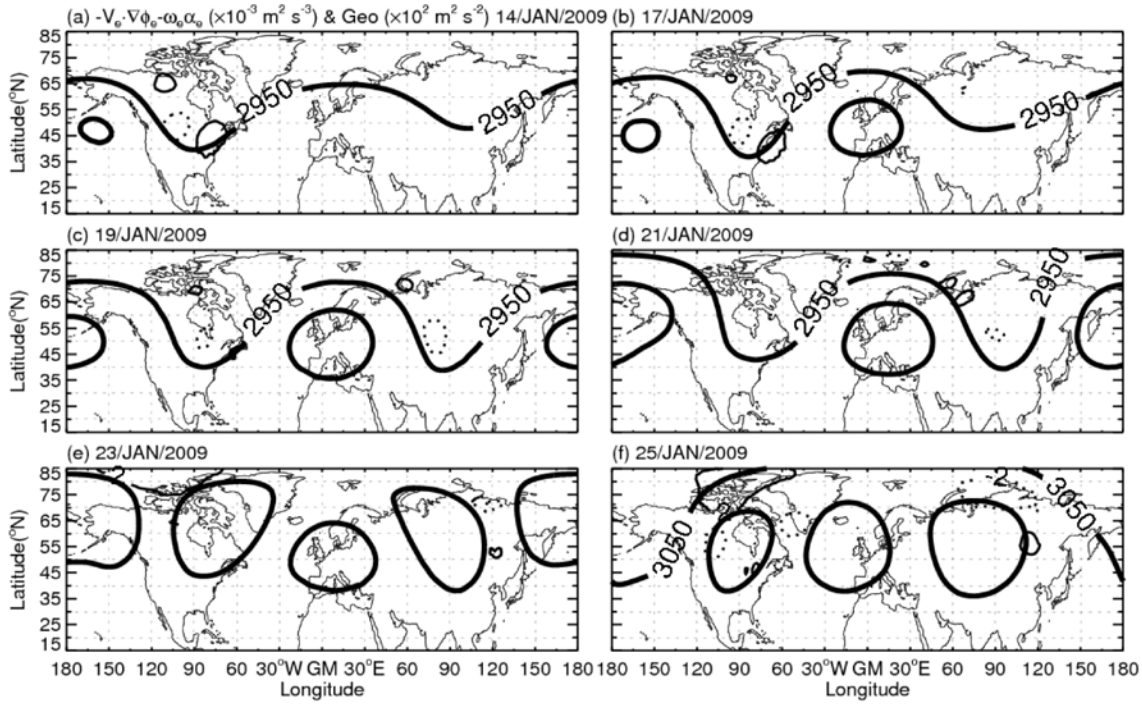

Fig. 5. Vertically averaged transient advection of geopotential height at 48-h intervals from 15 to 25 January 2009. The solid lines denote positive values and the dotted lines denote negative values. Contour interval is 2×10^{-3} m^2 s^{-3}. The contour of zero value is omitted. The geopotential values of 2950×10^2 m^2 s^{-2} and 3050×10^2 m^2 s^{-2} on 10 hPa are denoted by thick solid lines.

painen, 1978). Is this term interpreted as representing an energy conversion from K_m to K_e? Holopainen (1978) gave two expressions: $C(K_M, K_T)$, which was equal to the term mentioned above, and $C^*(K_M, K_T)$. Holopainen interpreted either $C(K_M, K_T)$ or $C^*(K_M, K_T)$ as the conversion of mean kinetic energy to transient kinetic energy. Which of the terms should be regarded as representing an energy conversion from K_m to K_e? Both terms were interpreted as the local feature of the energy conversion between mean and transient flow, but the local values of these two terms were different (Holopainen, 1978). Murakami (2011) developed a new diagnostic scheme for the atmosphere local energy analysis based on the concept of interaction energy (K_i) and its flux ($\boldsymbol{V}_e \cdot K_i$). By plotting interaction energy flux and box diagrams of the Lorenz energy cycle (Lorenz, 1955), the complete information about the three-dimensional structure of the energy interaction between mean and transient fields can be determined. If the K_e generation term (Eq. 9) is time averaged, the result is a part of the interaction kinetic energy flux divergence, expressed as C_2 by Murakami (2011), which means the energy conversion rates from K_i to K_e, expressed as $C(K_i, K_e)$ here. In this study, $C(K_i, K_e)$ was not time averaged and was also considered as a part of the interaction kinetic energy flux divergence, and consequently $C(K_m, K_i)$ was expressed as $C(K_m, K_i)$=div$(\boldsymbol{V}_e \cdot K_i) + C(K_i, K_e)$ [see Eq. (12c) in Murakami, 2011]. The quantities of $C(K_i, K_e)$ and $C(K_m, K_i)$ are plotted in Fig. 6, together with interaction energy flux vector.

On 9 January (Fig. 6a), over eastern Russia, K_m converted energy to K_i, and a part of K_i was transported eastward. When this K_i arrived in Canada, together with the K_i converted from K_e over Canada, it was transported through the Norwegian Sea and entered from northern Europe into Eurasia then converted energy to K_e over eastern Russia. When K_i passed through Eurasia, it obtained energy from mean flow over central Russia (Fig. 6a). Another part of K_i converted from K_m over eastern Russia was transported northeastward through the North Pole and then converted energy to K_m over Canada (Fig. 6a). Of course, there was a local conversion among K_i, K_m, and K_e over Canada and eastern Russia (Fig. 6a).

On 11 January (Fig. 6b), each conversion from one kinetic energy to the other increased over two continents more than those on 9 January, except $C(K_i, K_m)$ over Canada. The transport of K_i over Norwegian Sea did not pass through the Eurasia to eastern Russia but converted energy to K_m over western Russia on 11 January (Fig. 6b). This K_i flow remained

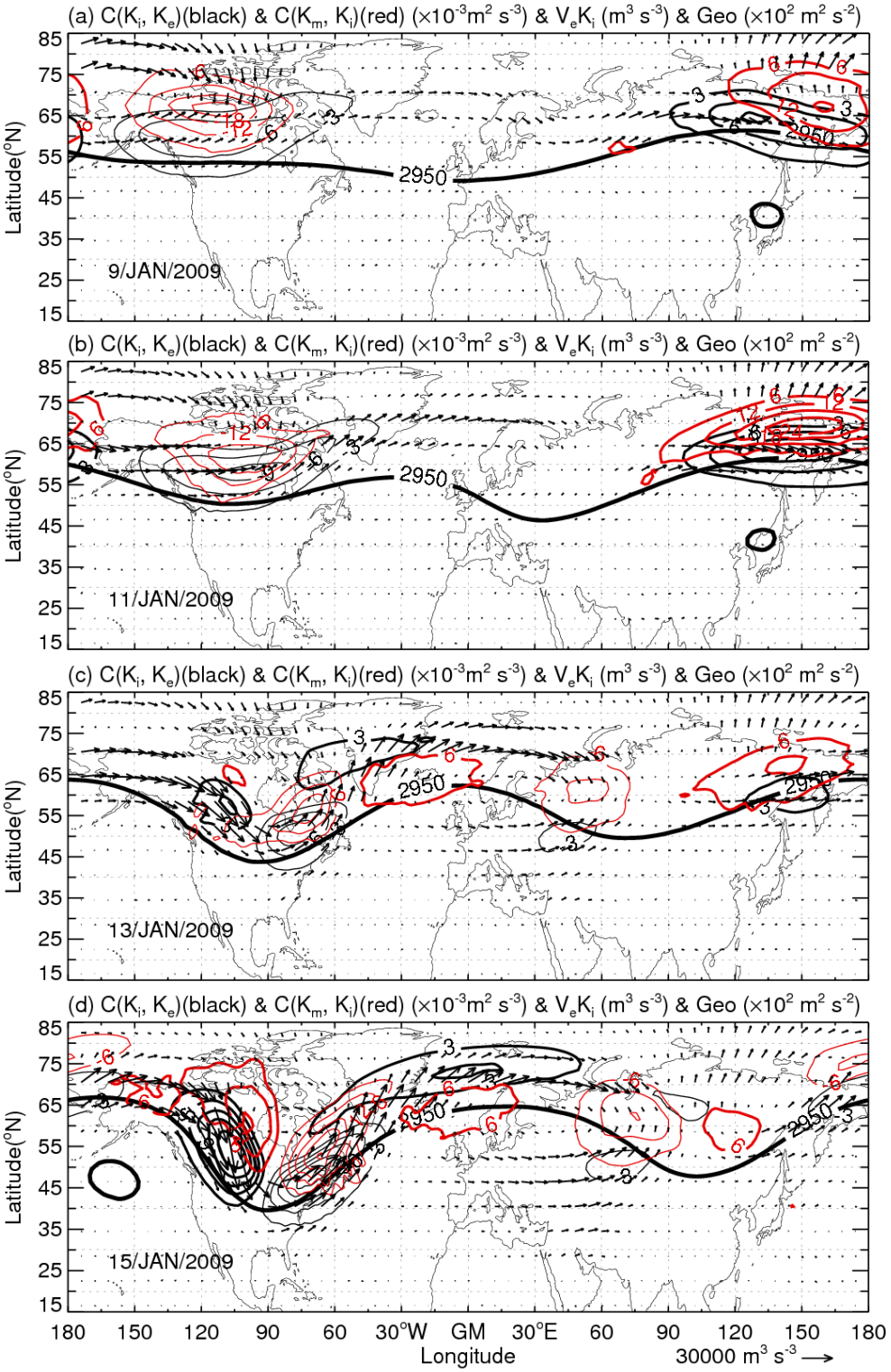

Fig. 6. Vertically averaged $C(K_\mathrm{i}, K_\mathrm{e})$ (black), $C(K_\mathrm{m}, K_\mathrm{i})$ (red) and the interaction energy flux vectors at 48-h intervals from 9 to 25 January 2009. The thick contour lines denote positive values and thin lines denote negative values. Contour interval is 3×10^{-3} m^2 s^{-3} for $C(K_\mathrm{i}, K_\mathrm{e})$ and 6×10^{-3} m^2 s^{-3} for $C(K_\mathrm{m}, K_\mathrm{i})$. The contour of zero value is omitted. Flux vectors are in units of 3×10^4 m^3 s^{-3} (see arrow below panel). The geopotential values of 2950×10^2 m^2 s^{-2} and 3050×10^2 m^2 s^{-2} on 10 hPa are denoted by boldfaced solid lines.

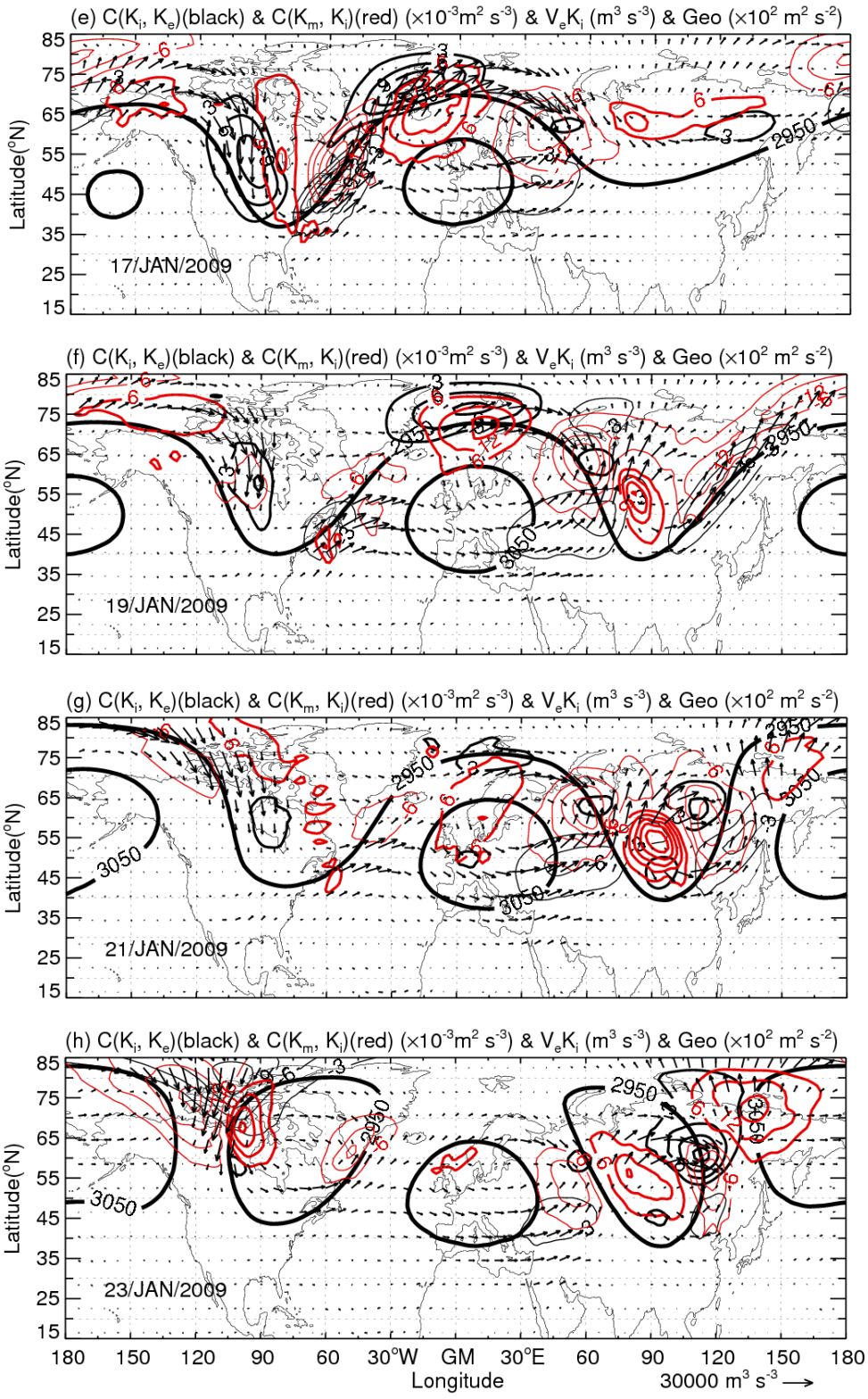

Fig. 6. Continued.

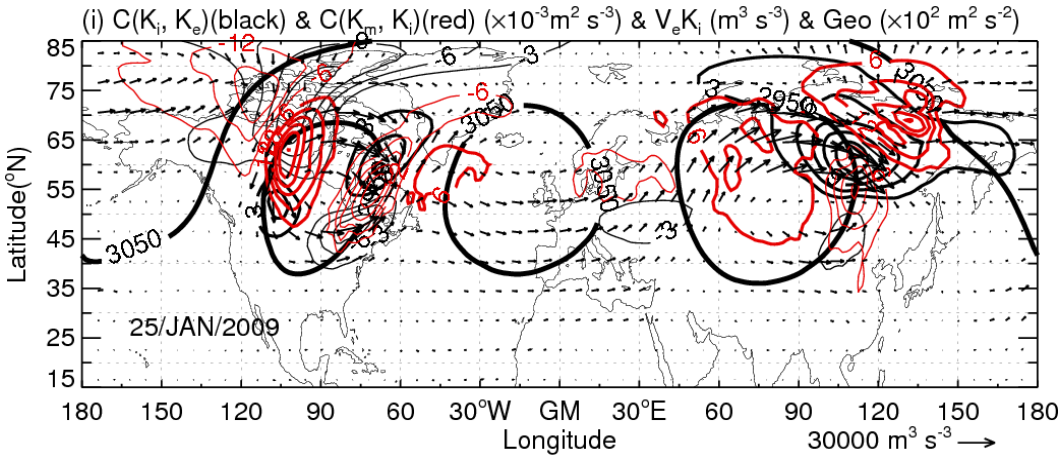

Fig. 6. Continued.

there before the SSW.

From 11 to 15 January (Figs. 6b–d), $C(K_i, K_m)$ and $C(K_e, K_i)$ over Canada decreased first and then increased and developed southeastward; finally, they were located over eastern North America. At the same time, $C(K_m, K_i)$ and $C(K_i, K_e)$ increased and developed southeastward over western North America. These southward developments were consistent with the deepening trough over North America. During this period, over the Norwegian Sea, $C(K_m, K_i)$ and $C(K_i, K_e)$ sharply increased and shifted slightly eastward, and over western Russia, $C(K_i, K_m)$ increased and shifted to central Russia. At the same time over eastern Russia, $C(K_i, K_e)$ decreased to $<3\times10^{-3}$ m^2 s^{-3}, and $C(K_m, K_i)$ decreased and shifted westward. Over the Chukchi Sea $C(K_i, K_m)$ developed during this period. A new K_i flow appeared, and the $C(K_m, K_i)$ developed over the Norwegian Sea. That is, K_i converted from K_m over Norwegian Sea entered into Eurasia from West Europe and converged over central Russia in which $C(K_i, K_m)$ was active (Figs. 6c–d).

On 15 January (Fig. 6c), over western North America, K_m converted energy to K_i and K_e gained energy from K_i, while over eastern North America, K_e converted energy to K_i and K_m gains energy from K_i. K_i flow, which originated from eastern Russia around (60°N, 120°E), passed through western North America from north to south and increased due to the transport of K_i from K_m into energy flow and then decreased due to the conversion from K_i into K_e. The energy flow changed direction over southern North America. Over this turning area, K_m slightly converted energy to K_i. This K_i flow continually passed through eastern North America from south to north and increased due to the support of K_i from K_e and then decreased due to the loss of K_i to K_e. When the energy flow passed through the Norwegian Sea, K_i converted energy to K_e. The growth of K_e over the Norwegian Sea was not only due to K_i flow from eastern North America but also to the northward transport of the K_i converted from K_m over the Norwegian Sea. The energy flowed continually through the Barents Sea into Russia and convergence over central Russia in which K_i converted energy to mean flow. The K_i converted from K_m over Norwegian Sea was also transported into Eurasia from West Europe and convergences over central Russia where $C(K_m, K_i)$ was active. So there were two main ducts of K_i energy flow. One was the K_i that originated from eastern Russia and passed through North America from north to south then turned north and through Norwegian and Barents Sea into central Russia. The other was the K_m that converted energy to K_i over the Norwegian Sea, and the K_i was transported into Eurasia from Western Europe and the convergences over central Russia where $C(K_m, K_i)$ was active (Fig. 6d).

From 15 to 17 January (Figs. 6d–e), the conversions among K_m, K_i, and K_e shifted eastward from western North America to central North America and $C(K_m, K_i)$ appeared over Alaska (Figs. 6d–e). $C(K_m, K_i)$ increased over the turning area of K_i flow, which indicates that there was more K_i into the K_i flow from mean flow. At the same time, $C(K_e, K_i)$ decreased and $C(K_i, K_m)$ held over eastern North America. Over the Norwegian Sea, more K_m converted energy to K_i, and more K_i, converted energy to K_e compared to 15 January (Figs. 6d–e). During this period, the high over Western Europe began to develop. This behavior resulted in more momentum flux between high and low pressure systems. On the basis of Eq. (9) here or Eq. (12c) in Murakami (2011), more kinetic energy converted from one type to another in this situation, as discussed previously. The conversions between K_m

and K_i over Eurasia shifted westward and increased, so $C(K_i, K_m)$ was located over western Russia, and $C(K_m, K_i)$ was located over central Russia on 17 January (Figs. 6d–e). Consequently, the third K_i flow was found over the Atlantic; that is, this K_i flow came from the turning area where $C(K_m, K_i)$ increased and also from convergences over western Russia to convert energy to the mean flow.

From 17 to 21 January (Figs. 6e–g), $C(K_m, K_i)$ shifted westward from Alaska to eastern Russia and $C(K_i, K_e)$ over central North America decreased. During this period, $C(K_m, K_i)$ shifted eastward from central North America to eastern North America and decreased. During the same period, $C(K_i, K_m)$ over central North America increased and developed northwestward and southward. Due to the decrease of $C(K_m, K_i)$ and the increase of $C(K_i, K_m)$ over North America, the K_i in energy flow decreased; hence, the $C(K_i, K_e)$ decreased over North America. At this time, $C(K_i, K_m)$ shifted eastward from eastern North America to the North Atlantic and sharply decreased. $C(K_e, K_i)$ over eastern North America sharply decreased and finally was $<3\times10^{-3}$ m^2 s^{-3} on 21 January. Due to these decreases, the K_i flow from the turning area to the Norwegian Sea sharply decreased then broke. $C(K_m, K_i)$ shifted slightly eastward over the Norwegian Sea to the western coast of Europe, decreasing and developing southward. $C(K_i, K_e)$ decreasd sharply and shifted eastward slightly. The decrease of $C(K_m, K_i)$ and $C(K_i, K_e)$ over the Norwegian Sea resulted in the decrease of the energy flow from the Norwegian Sea to western Russia. Over Western Europe around (50°N, 0°E) $C(K_m, K_i)$ increased, so when the energy flow from the turning area passed through Atlantic and this area to western Russia, it grew. During this period, kinetic energy conversions over North America decreased, and over Eurasia they increased. They may have resulted from the development of a trough over Eurasia and the eastward shift of the Western European high. Because the variations of the two systems can produce more momentum flux over Eurasia, the conversions of kinetic energy became more active over this continent. Because the Western European high eastward shifted and the trough over North America almost held, kinetic energy conversions over North America decreased. $C(K_i, K_m)$ developed southwestward from Arctic Ocean to eastern Russia. $C(K_m, K_i)$ increased and shifted slightly southward from central Russia to around (50°N, 90°E). $C(K_i, K_m)$ developed and shifted slightly eastward from western Russia to around (60°N, 60°E). After these variations of energy conversion, there were two obvious K_i flows between two continents before the major warming event. One was an energy flow from the Norwegian Sea, where K_m converted energy to K_i to western Russia around (60°N, 60°E) where K_i converted energy to K_m. The other was the K_i flow from the turning area where K_m converted energy to K_i passed through the North Atlantic and the western coast of Europe where K_i gained energy toward western Russia around (60°N, 60°E) to convert energy to the mean flow.

Compared to $C(K_i, K_m)$ and $C(K_m, K_i)$ with $C(K_i, K_e)$ and $C(K_e, K_i)$ over Eurasia, the variations of $C(K_i, K_e)$ and $C(K_e, K_i)$ were smaller during 17–21 January. $C(K_i, K_e)$ and $C(K_e, K_i)$ over western Eurasia on 17 January shifted eastward and then were located around (60°N, 60°E) and (50°N, 60°E) on 21 January, respectively. $C(K_i, K_e)$ over eastern Eurasia on 17 January decreased and shifted westward then increased, and finally were located around (60°N, 120°E) on 21 January. $C(K_e, K_i)$ over eastern Eurasia on 17 January increased and developed southwestward then decreased, finally located around (50°N, 120°E) on 21 January. Consequently, the conversion between K_i and K_e surrounded $C(K_m, K_i)$ around (50°N, 90°E).

From 23 to 25 January (Figs. 5h–i) the major warming event occurred over the North Pole. The conversions between K_i and K_m arranged regularly with positive and negative phases appeared alternately around the pole on 23 January. During this period, the conversions between K_i and K_m decreased over Eurasia but increased over North America. $C(K_i, K_e)$ over the two continents increased during this period, while $C(K_e, K_i)$ increased only over North America. There was only one K_i flow remaining; the K_i flow passed through the North Atlantic to western Russia on 25 January.

4. Time evolution of the interaction APE and its transient flux

In this section, the second term on the right-hand side of Eq. (7), the APE generation term and baroclinic conversion $\omega_e\alpha_e$, which represents a conversion between A_e and K_e, is discussed, because mean and transient advections described by Eq. (7) are analogous to those discussed with respect to K_e (Figs. 3 and 4). The APE generation term is shown in Fig. 7.

On 9 January (Fig. 7a), interaction APE (A_i) flowed poleward and eastward from eastern Russia to northern North America and then back to its initial position. Over this position, the mean flow providing energy to A_i and $C(A_m, A_i)$ was approximately one order of magnitude larger than $C(A_e, A_i)$. In this process, A_i converted energy to A_e over eastern Russia, and A_i gained energy from A_e over northern North America.

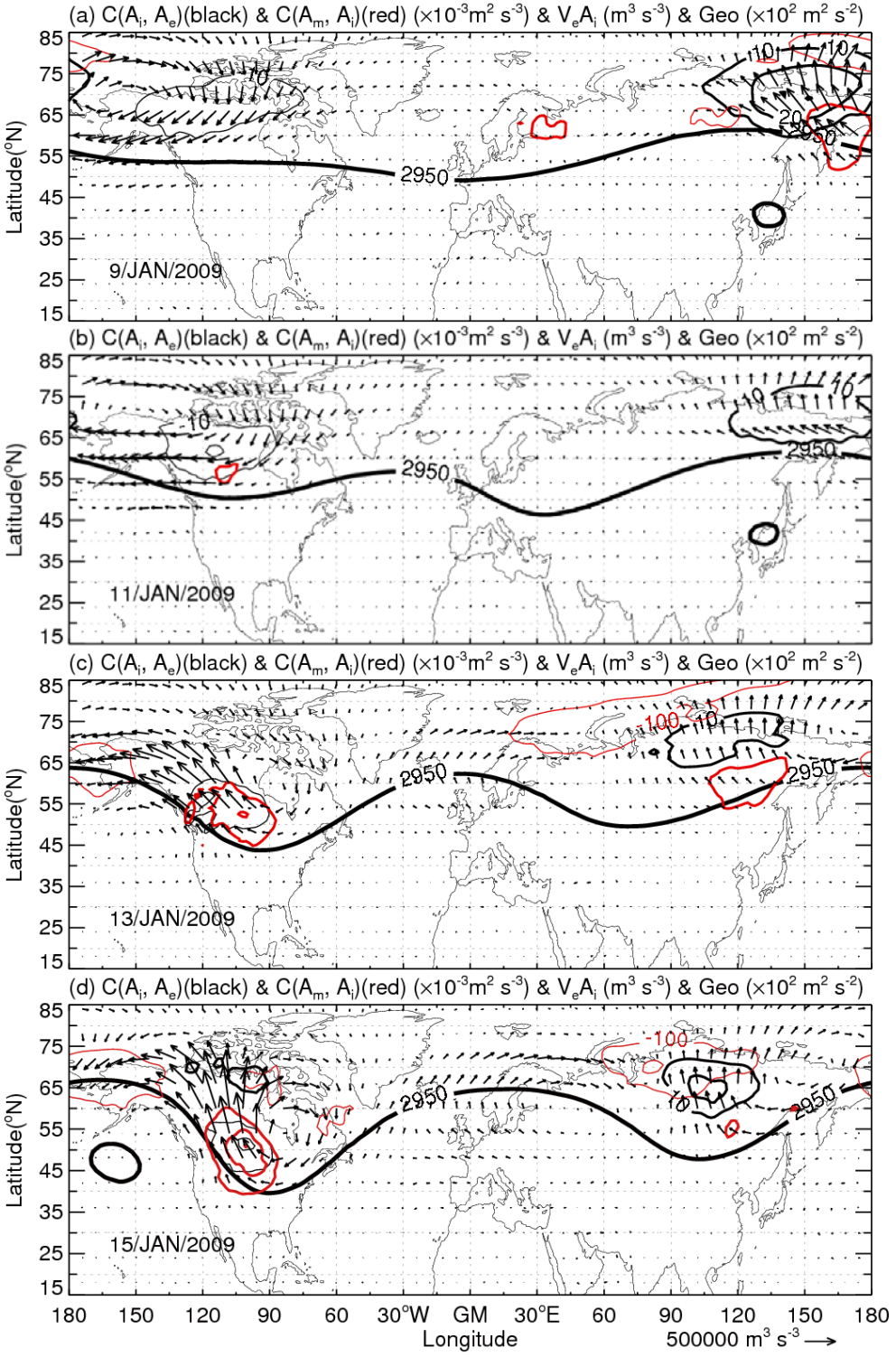

Fig. 7. Vertically averaged $C(A_\mathrm{i}, A_\mathrm{e})$ (black), $C(A_\mathrm{m}, A_\mathrm{i})$ (red) and the interaction energy flux vectors at 48-h intervals from 9 to 25 January 2009. The thick contour lines denote positive values and thin lines denote negative values. Contour interval is 10×10^{-3} m^2 s^{-3} for $C(A_\mathrm{i}, A_\mathrm{e})$ and 100×10^{-3} m^2 s^{-3} for $C(A_\mathrm{m}, A_\mathrm{i})$. The contour of zero value is omitted. Flux vectors are in units of 5×10^5 m^3 s^{-3} (see arrow below panel). The geopotential values of 2950×10^2 m^2 s^{-2} and 3050×10^2 m^2 s^{-2} on 10 hPa are denoted by boldfaced solid lines.

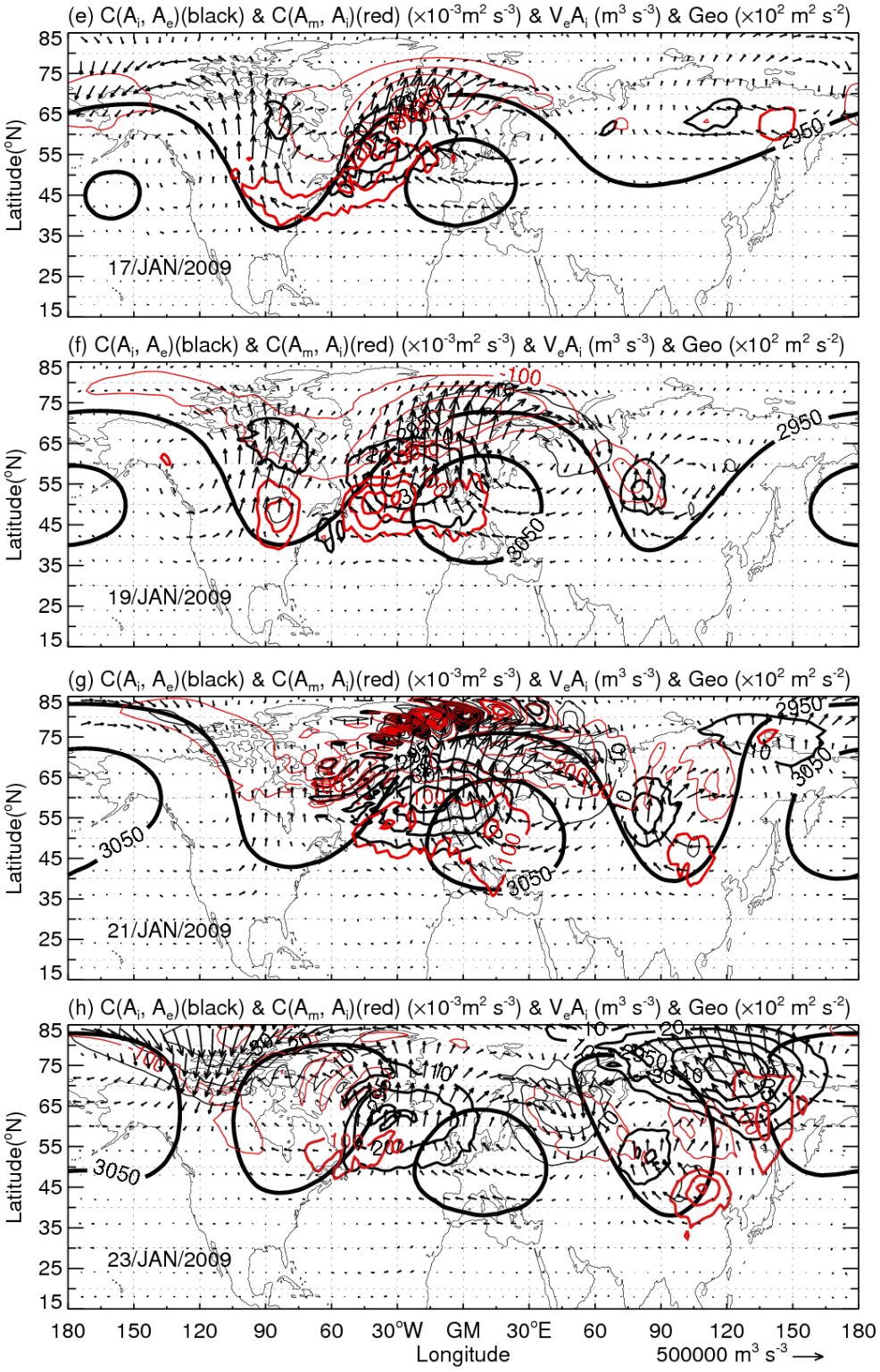

Fig. 7. Continued.

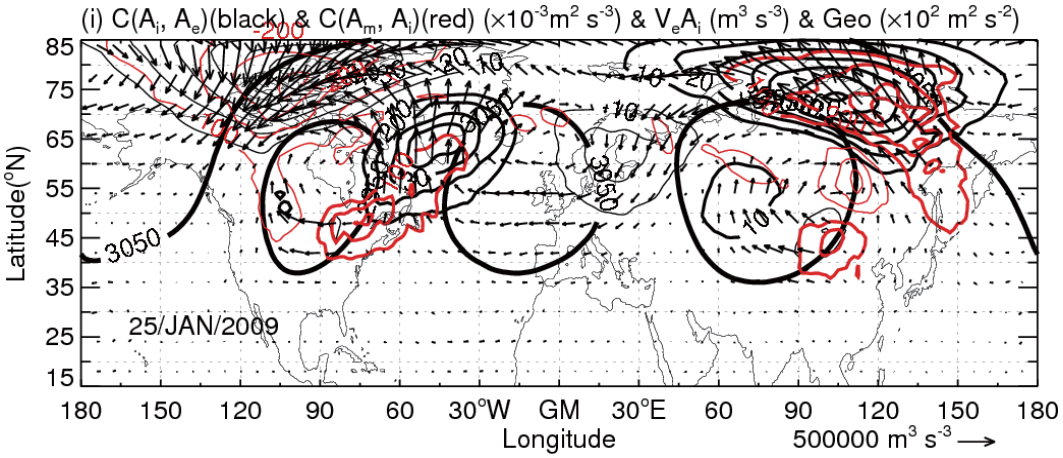

Fig. 7. Continued.

From 9 to 15 January (Figs. 7a–d), $C(A_e, A_i)$ shifted from northern North America to central North America. $C(A_m, A_i)$ increased over central North America, as the source of A_i. $C(A_i, A_m)$ increased over Alaska, as a sink of A_i. Because of the variation of source and sink regions of A_i, the A_i flow increased and changed direction to the northwest on 15 January over central North America (Figs. 7a–d). During the same period, $C(A_i, A_e)$ shifted from eastern Russia to central Russia and narrowed its control area; $C(A_m, A_i)$ shifted to central Russia and decreased, and over northern Russia $C(A_i, A_m)$ increased (Figs. 7a–d). Consequently, A_i flow changed position from eastern to central Russia (Figs. 7a–d).

From 15 to 19 January (Figs. 7d–f), over North America, $C(A_m, A_i)$ and $C(A_i, A_e)$ shifted eastward slightly. $C(A_i, A_m)$ shifted eastward from Alaska then connected $C(A_i, A_m)$, whose center was located in the Norwegian Sea. Due to these variations, A_i flow changed orientation from northwest on 15 January to northeast on 19 January over North America (Figs. 7d–f). The most remarkable characteristics were $C(A_m, A_i)$, $C(A_i, A_e)$, $C(A_i, A_m)$, and $C(A_e, A_i)$, which sharply increased over the North Atlantic and the Norwegian Sea during this period. Due to these dramatic variations, a strong A_i flow appeared from the North Atlantic to the Norwegian Sea, and conversion between one energy and another over this region became active. For instance, A_m converted energy to A_i over the North Atlantic. This converted A_i was transported northward and converted a part of energy to A_e then to A_m. Over the Norwegian Sea, A_e converted energy to A_i to compensate the loss of A_i flow, consequently, A_e increased over this region. At the same time, $C(A_i, A_m)$ and $C(A_i, A_e)$ shifted southwest from north Russia to central Eurasia (Figs. 7d–f). These active conversions of available potential energy may have resulted from the development of the Western European high. Because of the development of the high, more heat flux was produced over the area between the high and the North American trough. Consequently, the terms in the right-hand side of Eq. (7) here or Eq. (12c) in Murakami (2011) changed; that is, $C(A_i, A_e)$ and $C(A_m, A_i)$ changed.

From 19 to 21 January (Figs. 7f–g), over North America, $C(A_m, A_i)$ and $C(A_i, A_e)$ decreased to $<10\times10^{-3}$ m^2 s^{-3}. Over the North Atlantic $C(A_m, A_i)$ decreased and $C(A_i, A_e)$ increased. So, A_e continually increased over this region (Figs. 7f–g). On 21 January (Fig. 7g), drastic conversions among A_m, A_i, and A_e were found over the North Pole. During this period, the Western European high shifted slightly eastward, and the trough over Eurasia developed; this behavior may have resulted in the variation of heat flux over Eurasia. Finally, the conversions of available potential energy became more active over this continent.

From 21 to 25 January (Figs. 7g–i), $C(A_m, A_i)$ decreased first and then increased with westward shifting from the North Atlantic to eastern North America. The variation of $C(A_i, A_e)$ resulted from that of $C(A_m, A_i)$. The decrease of $C(A_i, A_m)$ to $<10\times10^{-3}$ m^2 s^{-3} over the Norwegian Sea and the shift of $C(A_e, A_i)$ toward northwestern Russia also resulted from the variation of $C(A_m, A_i)$. At the same time, over Eurasia and northern Canada energy conversion became more active than it had been previously (Figs. 7g–i). During this period, due to the development of the Aleutian high and cyclones over Eurasia and North America, more heat flux was produced, then more available potential energy was converted over the area between high and low pressure systems.

The $-\omega_e\alpha_e$ term, shown in Fig. 8, was approximately one order of magnitude less than APE genera-

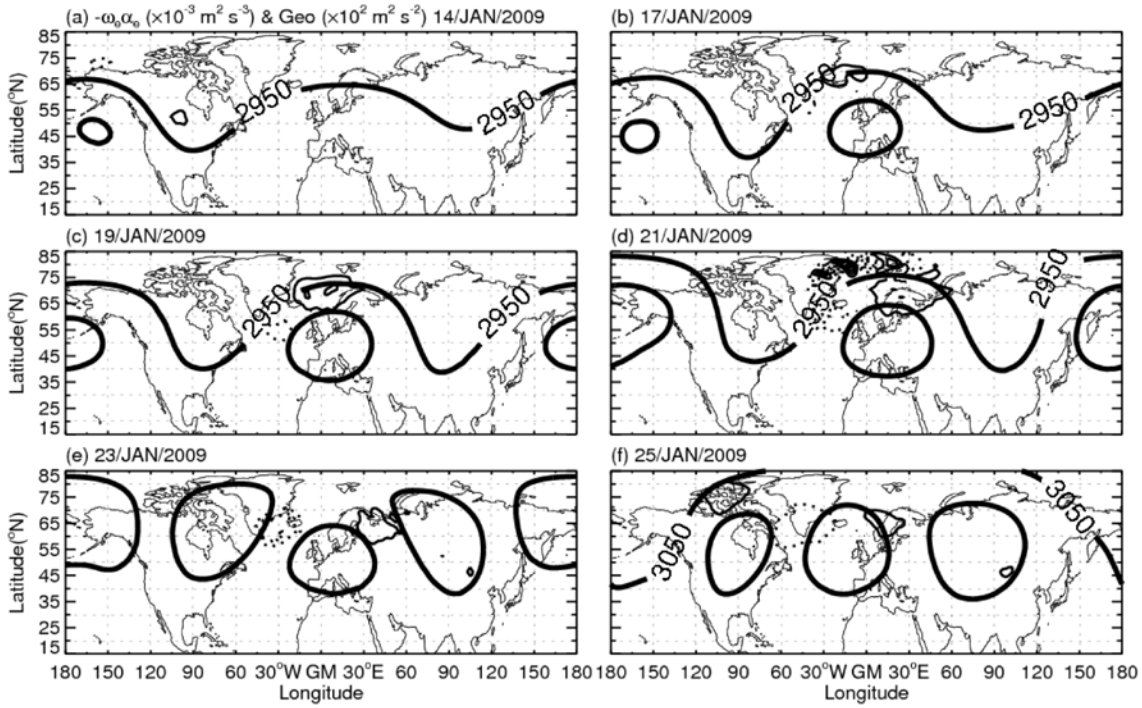

Fig. 8. Vertically averaged $-\omega_e\alpha_e$ at 48-h intervals from 17 to 25 January 2009. The solid lines denote positive values and dotted lines denote negative values. Contour interval is 2×10^{-3} m^2 s^{-3}. The contour of zero value is omitted. The geopotential values of 2950×10^2 m^2 s^{-2} and 3050×10^2 m^2 s^{-2} on 10 hPa are denoted by thick solid lines.

tion term and $<2\times10^{-3}$ m^2 s^{-3} before 17 January, so only the term from 17 to 25 January is shown in Fig. 8. This term is commonly interpreted as the conversion between transient kinetic energy and transient APE. This conversion was seen over the Norwegian Sea, converting A_e to K_e on 17 January (Fig. 8a). Before the major warming event, this conversion shifted eastward and was located over Western Europe (Figs. 8a–8d) and remained there during the warming event (Figs. 8d–e). The conversion from K_e to A_e can be found over the North Atlantic on 19 January and shifted to Greenland from 19 to 25 January. Over the northern Norwegian Sea, the conversions between A_e and K_e were active. A similar feature can be found at the same time in Fig. 7g. On the basis of this analysis, the baroclinic conversion $\omega_e\alpha_e$ was less important to the growth and decay of A_e or K_e during the SSW process.

5. Conclusion

The budget of transient available potential energy and kinetic energy were investigated using ECMWF Interim Reanalysis data during the SSW event of January 2009.

The SSW in January 2009 was characterized by the asymmetric variations of K_e and A_e between North America and Eurasia. The Western European high played important roles in the propagation of the energy from North America to Eurasia. When the Western European high appeared and shifted eastward, energy conversions increased and energy propagated from North America to Eurasia as a form of interaction energy flow. Energy was converted into interaction energy from mean flow, then was transported into transient energy from interaction energy. There were two main K_i flows between these two continents. One was the K_i flow that passed through North America and then through the Norwegian Sea into northern Russia. The other was the K_i flow that passed through the North Atlantic from the turning area over North America into Western Europe. The source of A_i flow was found over the North Atlantic. A_i flow passed through the North Atlantic and then through the Norwegian Sea into Eurasia.

The $\omega_e\alpha_e$ term, which was interpreted as the conversion between K_e and A_e, and the horizontal advection of geopotential height were approximately one order of magnitude less than K_e and A_e generation terms. Therefore, these terms were less important to

the growth and decay of K_e and A_e during this SSW event.

Acknowledgements. We are grateful to the ECMWF for making their respective datasets readily available online. This work was supported by the National Natural Science Foundation of China (Grant Nos. 40930950 and 40921160379) and the National Basic Research Program of China (Grant No. 2010CB428603).

REFERENCES

Andrews, D. G., J. R. Holton, and C. B. Leovy, 1987: *Middle Atmosphere Dynamics*. Academic Press, 489pp.

Baldwin, M. P., and T. J. Dunkerton, 2001: Stratospheric harbingers of anomalous weather regimes. *Science*, **294**, 581–584.

Dunkerton, T. J., and D. P. Delisi, 1986: Evolution of potential vorticity in the winter stratosphere of January–February 1979. *J. Geophys. Res.*, **91**(D1), 1199–1208.

Harada, Y., A. Goto, H. Hasegawa, N. Fujikawa, H. Naoe, and T. Hirooka, 2010: A major stratospheric sudden warming event in January 2009. *J. Atmos. Sci.*, **67**, 2052–2069.

Hirooka, T., T. Ichimaru, and H. Mukougawa, 2007: Predictability of stratospheric sudden warmings as inferred from ensemble forecast data: Intercomparison of 2001/02 and 2003/04 winters. *J. Meteor. Soc. Japan*, **85**, 919–925.

Holopainen, E. O., 1978: A diagnostic study on the kinetic energy balance of the long-term mean flow and the associated transient fluctuation in the atmosphere. *Geophysica*, **15**, 125–145.

Holton, J. R., and H.-C. Tan, 1980: The influence of the equatorial quasi-biennial oscillation on the global circulation at 50 mb. *J. Atmos. Sci.*, **37**, 2200–2208.

Julian, P. R., and K. Labitzke, 1965: A study of atmospheric energetics during January and February 1963 stratospheric warming. *J. Atmos. Sci.*, **22**, 597–610.

Kuroda, Y., 2008: Effect of stratospheric sudden warming and vortex intensification on the tropospheric climate. *J. Geophys. Res.*, **113**(D15110), doi: 10.1029/2007JD009550.

Labitzke, K., 1982: On the interannual variability of the middle stratosphere during the northern winters. *J. Meteor. Soc. Japan*, **60**, 124–139.

Labitzke, K., 1987: Sunspots, the QBO, and the stratospheric temperatures in the north polar region. *Geophys. Res. Lett.*, **14**, 535–537.

Labitzke, K., and H. van Loon, 1992: On the association between the QBO and the extratropical stratosphere. *J. Atmos. Terr. Phys.*, **54**, 1453–1463.

Labitzke, K., and H. van Loon, 1999: *The Stratosphere: Phenomena, History, and Relevance*. Springer-Verlag, 179pp.

Labitzke, K., M. Kunze, and S. Brönnimann, 2006: Sunspots, the QBO, and the stratosphere in the north polar region-20 years later. *Meteor. Z.*, **3**, 355–363.

Lorenz, E. N., 1955: Available potential energy of the maintenance of the general circulation. *Tellus*, **7**, 157–167.

Matsuno, T., 1971: A dynamical model of the stratospheric sudden warming. *J. Atmos. Sci.*, **28**, 1479–1494.

Muench, H. S., 1965: On the dynamics of the wintertime stratosphere circulation. *J. Atmos. Sci.*, **22**, 349–360.

Mukougawa, H., H. Sakai, and T. Hirooka, 2005: High sensitivity to the initial condition for the prediction of stratospheric sudden warming. *Geophys. Res. Lett.*, **32**(L17806), doi: 10.1029/2005GL022909.

Murakami, S., 2011: Atmospheric local energetics and energy interactions between mean and eddy fields. Part I: Theory. *J. Atmos. Sci.*, **68**, 760–768.

Murakami, T., 1965: Energy cycle of the stratospheric warming in early 1958. *J. Meteor. Soc. Japan*, **43**, 262–283.

Nakagawa, K. I., and K. Yamazaki, 2006: What kind of stratospheric sudden warming propagates to the troposphere? *Geophys. Res. Lett.*, **33**, L04801, doi: 10.1029/2005GL024784.

Palmer, T. N., 1981: Diagnostic study of a wavenumber-2 stratospheric sudden warming in a transformed Eulerian-mean formalism. *J. Atmos. Sci.,* **38**, 544–855.

Perry, J. S., 1967: Long wave energy processes in the 1963 sudden stratospheric warming. *J. Atmos. Sci.*, **24**, 537–550.

Plumb, R. A., 1983: A new look at the energy cycle. *J. Atmos. Sci.*, **40**, 1669–1688.

Reed, R. J., J. Wolfe, and H. Nishimoto, 1963: A special analysis of the energetics of the stratospheric sudden warming of early 1957. *J. Atmos. Sci.*, **20**, 256–275.

Simmons A, S. Uppala, D. Dee, and S. Kobayashi, 2007: ERA-Interim: New ECMWF reanalysis products from 1989 onwards. *ECMWF Newsletter*, **110**, 25–35.